Trap-Assisted Recombination via Integer Charge Transfer States in Organic Bulk Heterojunction Photovoltaics

Qinye Bao, Oskar Sandberg, Daniel Dagnelund, Simon Sandén, Slawomir Braun, Harri Aarnio, Xianjie Liu, Weimin M. Chen, Ronald Österbacka, and Mats Fahlman**

Organic photovoltaics are under intense development and significant focus has been placed on tuning the donor ionization potential and acceptor electron affinity to optimize open circuit voltage. Here, it is shown that for a series of regioregular-poly(3-hexylthiophene):fullerene bulk heterojunction (BHJ) organic photovoltaic devices with pinned electrodes, integer charge transfer states present in the dark and created as a consequence of Fermi level equilibrium at BHJ have a profound effect on open circuit voltage. The integer charge transfer state formation causes vacuum level misalignment that yields a roughly constant effective donor ionization potential to acceptor electron affinity energy difference at the donor–acceptor interface, even though there is a large variation in electron affinity for the fullerene series. The large variation in open circuit voltage for the corresponding device series instead is found to be a consequence of trap-assisted recombination via integer charge transfer states. Based on the results, novel design rules for optimizing open circuit voltage and performance of organic bulk heterojunction solar cells are proposed.

1. Introduction

With the rapidly rising energy conversion efficiency of up to 10%,[1,2] organic photovoltaic (OPV) devices such as polymer:fullerene bulk heterojunction (BHJ) solar cells are considered to be a promising renewable-energy source with the potential of high throughput, low manufacturing cost, light weight, and mechanical flexibility.[3,4] In order to further optimize and improve the efficiencies so as to enable their successful commercialization, significant efforts are made to increase two particular photovoltaic parameters: short circuit current density (J_{sc}) and open circuit voltage (V_{oc}).[5–8] The energy difference between the hole-transporting level of the donor and the electron-transporting level of the acceptor heavily influences the V_{oc} and can be seen as an upper limit to what can be achieved in the device. Strategies to increase the V_{oc} typically have focused on synthesis of new polymers and/or new acceptor/fullerene derivatives so as to achieve optimal donor (D)–acceptor (A) energy level offsets.[9–11] More recently, a significant influence of photogenerated donor–acceptor charge transfer (CT) complexes on V_{oc} has been demonstrated,[12,13] but strategies for V_{oc} (and overall efficiency) improvement based on this effect are less explored. In general, the V_{oc} is found to be proportional to the incoming light intensity I such that $eV_{oc} \propto n_s kT \ln(I)$, where n_s is a prefactor (sometimes referred to as the light ideality factor), usually $1 < n_s < 2$.[14]

Ultraviolet photoelectron spectroscopy (UPS), inverse photoemission spectroscopy (IPES) and cyclic voltammetry (CV) are typically used to measure the energies of the hole- and electron transporting levels, with CV being most commonly used due to its relative simplicity and low cost. Knowledge of the (bulk) transport levels does not enable the determination of electrode and BHJ energetics, however, as a potential step is often formed at metal/organic and organic/organic interfaces modifying the relative position of the energy levels at either side of the interface,[15] even for weakly interacting physisorbed interfaces such as those typically found in a BHJ solar cell.[16–20]

It's proposed that the energy level alignment at weakly interacting metal/organic and organic/organic interfaces and in multilayer stacks can be predicted by the Integer Charge Transfer (ICT) model[16,21,22] where the relation between the original Fermi level of a surface and the so-called pinning energies ($E_{ICT+,-}$) of the organic semiconductor (OS) overlayer plays a key role. The E_{ICT+} (E_{ICT-}) energy of the positive (negative) ICT state relates to the smallest energy required to take away one electron (the largest energy gained from adding one electron) from (to) the OS molecule at an interface producing a fully relaxed state, where screening from the environment and the Coulombic interaction with the opposite charge across the

Q. Bao, Dr. S. Braun, Dr. X. Liu, Prof. M. Fahlman
Division of Surface Physics and Chemistry
Department of Physics
Chemistry and Biology
Linköping University
SE-58183, Linköping, Sweden
E-mail: qinba@ifm.liu.se; mats.fahlman@liu.se
Dr. O. Sandberg, Dr. S. Sandén, Dr. H. Aarnio, Prof. R. Österbacka
Center for Functional Materials
Department for Natural Sciences
Åbo Akademi University
FI-20500, Turku, Finland
Dr. D. Dagnelund, Prof. W. M. Chen
Division of Functional Electronic Materials
Department of Physics
Chemistry and Biology
Linköping University
SE-58183, Linköping, Sweden

DOI: 10.1002/adfm.201401513

interface are included.[23] These energies hence are related to but differ from the bulk ionization potential (IP) and electron affinity (EA) of the OS, that is, the polaronic transport states, see Figure S1 in the Supporting Information and described in more detail elsewhere.[17,23–25] Here we stress that the E_{ICT+} (E_{ICT-}) are located further into the gap compared to the free bulk polarons of the material, as the positive and negative polarons formed in the ICT-process are Coulombically bound at the interface by the opposing charge. We also stress that the ICT states are formed spontaneously to equilibrate the Fermi level at a heterojunction and are thus not photogenerated.

The pinning energies, also accessible by density functional theory,[24] can be applied to determine the energetics at the various interfaces in a BHJ solar cell and the possible existence of ICT states formed by spontaneous charge transfer at the BHJ interface,[17] the latter which can enhance the transformation of excitons into free charge carriers at the (bulk) heterojunction.[26,27] The effect, if any, of ICT states on V_{oc} has yet to be explored, however.

In polymer:fullerene BHJ solar cells, because the archetypical fullerenes C_{60}/C_{70} themselves are prone to aggregation and difficult to process with polymer donors, the monoadduct fullerene derivatives $PC_{60}BM$ and $PC_{70}BM$ widely dominate in terms of choice of acceptor material.[4,7,28,29] Recently, other fullerene derivatives with multiadducts with smaller EA energies have been introduced in BHJ device to increase the donor IP – acceptor EA energy difference and thereby enhance output performance by raising V_{oc}.[30–32] In this paper, we use UPS to systematically map out the occupied electronic structure and universal pinning energies of a series of fullerenes: $C_{60/70}$, $PC_{60/70}BM$, $BisPC_{60}BM$, $TrisPC_{60}BM$ and $IC_{60}BA$. The formation of ICT states at rr-P3HT:fullerene BHJs is addressed and the effect on V_{oc} is commented upon using modelling and device data from literature. In Figure S2 the chemical structure and in Figure S3 the frontier occupied electronic structure of fullerene and its derivatives considered in this study are exhibited (see Supporting Information).

2. Results and Discussion

Figure 1a displays the dependences of the work function of fullerene-coated substrates, $\Phi_{org/sub}$, on the work function of the original bare substrates, Φ_{sub}. Two distinct slope $S = 0$ regions are clearly observed, separated by an $S = 1$ region, as predicted by the ICT model. When the Φ_{sub} is smaller than the E_{ICT-} of a particular fullerene derivative, electrons spontaneously tunnel from the substrate into the fullerene molecules until equilibrium is reached, causing the formation of a potential step and pinning the Fermi level to the negative integer charge transfer state. The E_{ICT-} values corresponding to C_{60}, C_{70}, $PC_{60}BM$, $PC_{70}BM$ $bisPC_{60}BM$, $trisPC_{60}BM$, and $IC_{60}BA$ fullerenes are 4.57, 4.65, 4.31, 4.35, 4.12, 3.95, and 4.05 eV, respectively, as derived from Figure 1a. For Φ_{sub} greater than the E_{ICT+}, spontaneous electron transfer occurs from the fullerene molecules to the substrate, creating a potential step that downshifts the vacuum level and the Fermi level is pinned to the positive integer charge transfer state of the fullerene. The E_{ICT+} values of the fullerene derivatives are estimated from Figure 1a as 5.55, 5.48, 5.32, 5.22, 5.08, 4.95, and 5.15 eV, respectively. In the transition region ($S = 1$) between the negative and positive pinning regime, the $\Phi_{org/sub}$ of fullerenes is equal to Φ_{sub}, which means that no spontaneous charge transfer across interface and vacuum level (VL) alignment holds. For $trisPC_{60}BM$, there is a displacement in $\Phi_{org/sub}$ of ≈0.2 eV away from the "ideal" VL alignment behavior as shown in Figure 1a. We tentatively attribute the effect to preferential ordering of $trisPC_{60}BM$ molecules, see Figure S5 and discussion in the Supporting

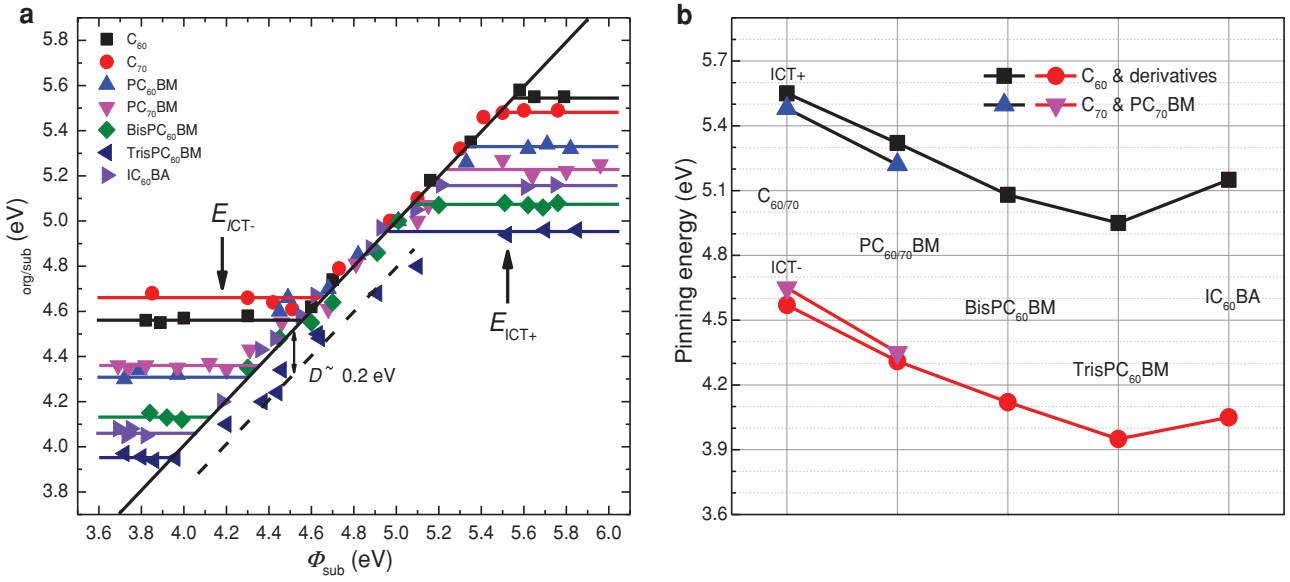

Figure 1. Universal pinning energies of a series of fullerenes. a) Dependences of the work function of C_{60}, C_{70}, $PC_{60}BM$, $PC_{70}BM$, $BisPC_{60}BM$, $TrisPC_{60}BM$, and $IC_{60}BA$ coated substrates via solution process, $\Phi_{org/sub}$, on the work function of bare substrate, Φ_{sub}. b) Distribution of the pinning energies of the fullerenes with increasing the number of adducts. E_{ICT+}: positive pinning energy (eV); E_{ICT-}: negative pinning energy (eV); D: the downshift energy of ≈0.2 eV away from the "ideal" vacuum level alignment behavior.

Table 1. Summary of positive/negative pinning energy ($E_{ICT+/-}$), ionization potential (IP), electronic affinity (EA) of fullerenes, Δ: interface potential step obtained from difference between fullerene E_{ICT-} and rr-P3HT E_{ICT+} (≈4.0 eV), $\Delta E_g^{DA} = IP_D - EA_A$: the difference between the donor IP (rr-P3HT ≈ 4.6 eV) and (fullerene) acceptor EA, $\Delta E_{g,eff}^{DA} = IP_D - EA_A + \Delta$: the difference between the donor IP and acceptor EA including the contribution from vacuum level misalignment at the BHJ, V_{oc} of devices with a structure of ITO/PEDOT: PSS/rr-P3HT:fullerene/LiF/Al and n_s: a prefactor related to the dominating recombination process in the rr-P3HT:fullerene blend (all n_s values obtained from Tromholt, et al.)[46]

Fullerene	E_{ICT+}	E_{ICT-}	IP	EA	Δ	ΔE_g^{DA}	$\Delta E_{g,eff}^{DA}$	V_{oc}	n_s
C_{60}	5.55	4.57	6.35	3.98[47]	0.57	0.62	1.19	0.46[46]	1.5
C_{70}	5.48	4.65	6.30	3.98	0.65	0.62	1.27	0.32[46]	1.61
$PC_{60}BM$	5.32	4.31	6.10	3.80[47]	0.31	0.8	1.11	0.62[48]	1.42
$PC_{70}BM$	5.22	4.35	5.90	3.80	0.35	0.8	1.15	0.63[48]	1.56
$BisPC_{60}BM$	5.08	4.12	5.95	3.60[49]	0.12	1.0	1.12	0.72[46]	1.42
$TrisPC_{60}BM$	4.95	3.95	5.85	3.50[50]	0	1.1	1.1	0.81[30]	–
$IC_{60}BA$	5.15	4.05	5.93	3.57[51]	0.05	1.03	1.08	0.86[31]	1.28

The IPs were measured by ultraviolet photoelectron spectroscopy (UPS) and the cited EA values are from inverse photoemission spectroscopy (IPES) studies, see further discussion in the Supporting Information. EA values reported by IPES measurements scatter over a large range, e.g., for $PC_{60}BM$ ≈ 0.35 eV,[47,52–54] due to the inherent problems of the technique such as sample damage and comparatively low energy resolution. In the situations of ambiguity, we have used literature cyclic voltammetry measurements on the same systems to try to reconcile the different values into the ones given. For C_{70}, we use the EA of C_{60} as cyclic voltammetry show that the reduction potential is ≈ identical.[55] $E_{ICT+/-}$, IP, EA, ΔE_g^{DA} and $\Delta E_{g,eff}^{DA}$ are shown in units of eV, and V_{oc} is shown in units of V.

Information. Figure 1b shows the evolution of the fullerene $E_{ICT+,-}$ with increasing number of adducts. For the different types of fullerene cages, the E_{ICT-} values of $C_{60}/PC_{60}BM$ are slightly smaller than that of the corresponding $C_{70}/PC_{70}BM$ and the E_{ICT+} slightly larger. The respective IP, EA, and $E_{ICT+,-}$ for the fullerene series are listed in **Table 1**.

Using the $E_{ICT+,-}$ values one can then estimate which electrode work function are needed to pin the Fermi level at the respective contact, at which point the V_{oc} is no longer limited by the work function difference of the electrodes: the anode work function should be equal or greater than the donor polymer E_{ICT+} and the cathode work function equal or smaller than the fullerene E_{ICT-}. Typically PEDOT:PSS is used as the anode material and though the work function depends on the particular formulation it is often around 5.1 eV,[10] significantly larger than the measured E_{ICT+} of most of the donor polymers. The PEDOT:PSS interface thus is expected to feature Fermi level pinning to the donor polymer E_{ICT+}, as desired. At the cathode side, an electrode work function smaller than the acceptor fullerene E_{ICT-} is needed to achieve a pinned interface. From the device characteristics of ITO/PEDOT:PSS/MDMO-PPV:$PC_{60}BM$/cathode (LiF/Al, Ag, Au, and Pd) reported by Mihailetchi,[33] the dependence of V_{oc} on different cathode work function has been explored and for Ag, Au, and Pd cathodes, there is a significant decrease in V_{oc} obtained compared to the case of the low work function LiF/Al contact that is pinned (0.9 V for LiF/Al down to 0.4 V for Pd). Such a decrease is expected from our results as the E_{ICT-} of $PC_{60}BM$ is ≈4.3 eV and the higher work function Ag, Au or Pd hence will not provide a pinned contact, unlike LiF/Al whose (process-dependent) work function is ≈3.6 eV or lower.[34]

For the case of pinned electrode contacts, the V_{oc} is suggested to be controlled by the donor/acceptor blend, though recent literature makes clear that donor IP–acceptor EA energy difference (ΔE_g^{DA}) alone does not adequately describe the V_{oc}.[12,13] The influence of the D/A blend properties, including the effects from ICT states (if any), thus can be explored using data from ITO/PEDOT:PSS/rr-P3HT:fullerene (C_{60}, C_{70}, $PC_{60}BM$, $PC_{70}BM$, $bisPC_{60}BM$, $trisPC_{60}BM$, and $IC_{60}BA$)/LiF/Al devices, where the LiF/Al cathode will pin to the E_{ICT-} of all fullerenes we studied here and the PEDOT:PSS anode will likewise pin to the E_{ICT+} of rr-P3HT, ≈4.0 eV.[26]

We first look at the effect of ICT states at the BHJ that according to the ICT model may form to ensure Fermi level equilibrium at interfaces. Inserting an intrinsic dipole layer at a donor–acceptor junction forming a trilayer will increase the effective $IP_D - EA_A$ difference ($\Delta E_{g,eff}^{DA}$) and hence the V_{oc} for the case of a dipole layer with the negative side at the acceptor and decrease the $\Delta E_{g,eff}^{DA}$ (and hence the V_{oc}) for the case of a dipole layer with the negative side at the donor, see Figure S6a,b in Supporting Information.[35] The effect on V_{oc} is different if the dipole shift is introduced through the formation of ICT states as per the ICT model (see supplementary background), however, as we will show using V_{oc} values from the ITO/PEDOT:PSS/rr-P3HT:fullerene/LiF/Al device series, the corresponding donor IP (≈4.6 eV for rr-P3HT) and (fullerene) acceptor EA values as well as BHJ potential steps derived from the $E_{ICT+,-}$ values, see Table 1.

As is evident from Table 1, failing to account for vacuum level misalignment at the BHJ (interface potential steps) can produce severe errors in the estimation of the effective ΔE_g^{DA}, that is, $\Delta E_{g,eff}^{DA}$ in Table 1, as for some fullerene:rr-P3HT combinations there is a large interface potential step. Note also that for this particular series, the V_{oc} seems largely independent of the $\Delta E_{g,eff}^{DA}$ values (the two lowest $\Delta E_{g,eff}^{DA}$ actually produces the two highest V_{oc}). Furthermore, the $\Delta E_{g,eff}^{DA}$ values show only a small variation (≈1.1–1.25 eV) despite the large variation in (bulk) donor IP–acceptor EA energies (ΔE_g^{DA}), as a decrease in acceptor EA also causes a decrease in acceptor E_{ICT-} and thus a decrease in the Δ. Modifying the fullerene EA in regards to a particular donor IP (or modifying a donor IP in regards to a particular fullerene EA) hence is not expected to significantly change $\Delta E_{g,eff}^{DA}$ as long as the BHJ is in the pinned regime (the case for the rr-P3HT series, with the exception of $trisPC_{60}BM$, though the 0.05 eV difference between the $E_{ICT+,-}$ levels are within the error margin of the measurement). This obviously

also holds true for the effective donor EA–acceptor EA relation ($\Delta E^{DA}_{g,eff}$). The increase in V_{oc} obtained by introducing fullerene derivatives with multiadducts with smaller EA energies hence does not increase the effective donor IP–acceptor EA energy difference unlike previously believed[30–32] and the cause for the enhanced V_{oc} must be found elsewhere.

To better understand the processes that influence on V_{oc}, we build upon recent models that assume direct bimolecular recombination between free charge carriers to obtain the following expression (analysis based on a pn-junction approach is given in the Supporting Information):[14,36]

$$\begin{aligned} eV_{oc} &= \Delta E^{DA}_{g,eff} - kT\ln\left(\frac{\beta N_c N_v}{G}\right) \\ &= \Delta E^{DA}_{g} + \Delta - kT\ln\left(\frac{\beta N_c N_v}{G}\right) \end{aligned} \quad (1)$$

where ΔE^{DA}_{g} is as noted the difference between the IP of the donor and the EA of the acceptor before junction formation, Δ is a factor that accounts for effects such as vacuum level misalignments at the BHJ that modify the activation energy gained from ΔE^{DA}_{g}, $\Delta E^{DA}_{g,eff} = \Delta E^{DA}_{g} + \Delta$ is then the effective energy gap between the donor IP and acceptor EA taking into account vacuum level misalignment, and N_c and N_v are the effective density of transport (polaron) states, and β is the bimolecular recombination coefficient.[37] The free polaron generation rate G, is usually related to the light intensity as $G \propto I^{\alpha}$, where α is close to unity. The probability for CT complexes, formed upon direct recombination between free carriers (polarons), to dissociate back to free carriers has been effectively included in the bimolecular recombination coefficient β. It can be shown that Equation (1) is equivalent to the more commonly used formula:

$$eV_{oc} = kT\ln\left(\frac{J_{sc}}{J_o} + 1\right) \quad (2)$$

where J_{sc} is the short-circuit current density and J_0 is reverse dark saturation current density (see Supporting Information).

If a large amount of recombination centers or trapped carriers exist, trap-assisted recombination may also occur at the D/A BHJ interface, which further modifies Equation 1. This process is usually taken to follow Shockley-Read-Hall (SRH) recombination and has in rr-P3HT:PC_{60}BM OPVs been attributed to involve localized states in the tails of the rr-P3HT valence band and PC_{60}BM conduction band acting as traps and consequently recombination sites.[38] Trap-assisted recombination via occupied ICT states, if present, will also occur as the donor E_{ICT+} is situated above the free positive polaron and the acceptor E_{ICT-} is situated below the free negative polaron,[16,23,24] see **Figure 2**. If ICT states have been created as per the ICT model, a free negative (positive) polaron in the fullerene (polymer) thus may recombine with a E_{ICT+} (E_{ICT-}) related positive (negative) polaron located at the interface in the polymer (fullerene) as illustrated in Figure 2. If trap-assisted recombination via these states becomes comparable to the direct bimolecular recombination one finds (see Supporting Information Section 2.5):

$$\begin{aligned} eV_{oc} &= \Delta E^{DA}_{g,eff} \\ &-kT\ln\left(\frac{\beta N_c N_v + \beta_{SRH} N_{ICT}\sqrt{N_c B_v}\exp\left(\frac{\Delta E^{DA}_{g,eff} - eV_{oc}}{2kT}\right)}{G}\right) \\ &\approx \Delta E^{DA}_{g,eff} - n_s kT\ln\left(\frac{C_o(\Delta)}{G}\right) \end{aligned} \quad (3)$$

where N_{ICT} is the density of ICT states and C_o is a function of Δ. As all recombination essentially occur at the interfaces, in case of a large amount of ICT states trap-assisted recombination via these states is expected. The prefactor n_s increases with increasing trap-assisted recombination and is thus related to the dominating recombination process, the two extreme cases being $n_s = 1$ for direct bimolecular recombination and $n_s = 2$ for trap-assisted recombination. To a first approximation: $\frac{\Delta}{q} \sim \frac{qN_{ICT}}{\varepsilon\varepsilon_0}\delta^2$, where δ is the dipole thickness. Consequently, if the dipole Δ is large, N_{ICT} also is large and the trap-assisted recombination is expected to be more prominent.

The existence of ICT states at the D/A interface occur when $E_{ICT+,D} \leq E_{ICT-,A}$ and ICT states act as sites for recombination that reduce the V_{oc}. On the other hand, previous studies suggests that the generation of free charges at the D/A interface is enhanced by the type of interface dipole generated by the ICT states.[26,27] Furthermore, the ICT states will populate the most easily oxidized polymer chains or chain segments on the rr-P3HT side of the heterojunction (most likely to undergo structural relaxation), and the most easily reduced PC_{60}BM molecules at the other side (see Supporting Information). In this way, the most tightly bound sites where charge transfer electron-hole pairs could be created at the interface are already occupied in the (dark) ground state and are consequently not available to participate in the exciton dissociation process following a photon absorption event, thus enhancing the percentage of excitons converted into free charges.[39,40] Hence, there is likely a trade-off in terms of ICT state density as the presence of ICT states enhance the generation of free charges at the BHJ, but also enhance the recombination of free charges at the BHJ. From the rr-P3HT:fullerene series studied here it seems that the sweet spot occurs for $E_{ICT-,A} \approx E_{ICT+,D}$ (e.g., rr-P3HT:IC_{60}BA). We now test this hypothesis by measuring the E_{ICT+} and IP of a set of high-performing donor polymers in literature and comparing the $\Delta E^{DA}_{g,eff}$ with measured V_{oc} from literature, see **Figure 3**, Figure S4 and Table S1. Striking in Figure 3 is that many of the high performing polymer:fullerene blends precisely fall in the region (green in top panel of Figure 3) where $E_{ICT-,A} = E_{ICT+,D} \pm 0.05$ eV and where the $V_{oc\ loss}$ defined as the deviation from the ideal V_{oc} ($\Delta E^{DA}_{g,eff}$) in the measured V_{oc} $\left(eV_{ocloss} = \Delta E^{DA}_{g,eff} - eV_{oc}\right)$ is at its minimum, in agreement with our design rule. Note also that just a small deviation in either direction cause a significant jump in $V_{oc\ loss}$.

In terms of Equation 1 and Equation 3, $V_{oc\ loss}$ can be rewritten as

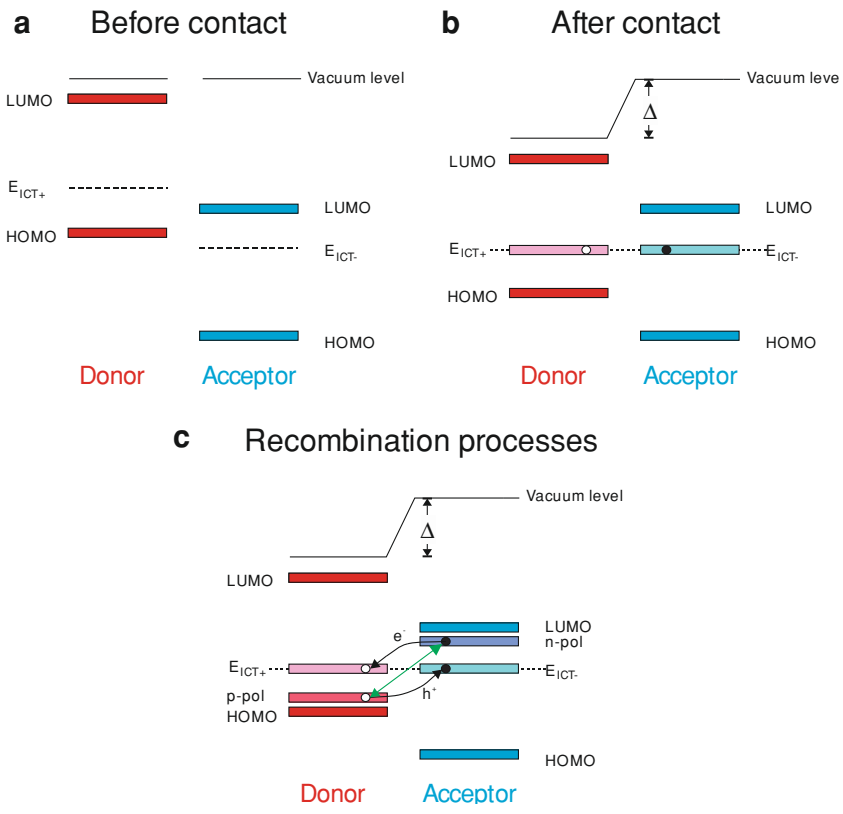

Figure 2. Energy level alignment diagrams for a donor–acceptor system before and after BHJ formation with a dipole shift introduced through ICT states. a) Before contact. b) The donor E_{ICT+} is less the acceptor E_{ICT-}, causing Fermi level equilibrium through spontaneous formation of ICT states at the interface and the formation of a potential energy step (Δ) upon contact. c) During OPV operation, free negative polarons (n-pol) in the acceptor may recombine with the opposite-charged interface polarons (E_{ICT+}) in the donor as the free n-polarons are situated above the donor E_{ICT+}. Correspondingly, free positive polarons (p-pol) in the donor may recombine with the opposite-charged interface polarons (E_{ICT-}) in the acceptor as the free p-polarons are situated below the acceptor E_{ICT-}. Direct bimolecular recombination of free polarons is depicted with a green arrow. The highest occupied molecular orbital (HOMO) and lowest unoccupied molecular orbital (LUMO) of the donor (red) and acceptor (blue) are also depicted.

$$eV_{ocloss} = \begin{cases} kT\ln\left(\frac{\beta N_c N_v}{G}\right), \text{when } E_{ICT-,A} - E_{ICT+,D} < 0 \\ n_s kT\ln\left(\frac{C_o(\Delta)}{G}\right), \text{when } E_{ICT-,A} - E_{ICT+,D} > 0 \end{cases} \quad (4)$$

To the right of the green region in Figure 3 there is no (dark) integer charge transfer at the bulk heterojunction ($E_{ICT+,D} > E_{ICT-,A}$ and $\Delta = 0$). Consequently, no trap-assisted recombination via ICT states is expected and the dominating recombination process is bimolecular ($n_s = 1$). As the deviation of the fraction G/β in these blends is expected to be less than a factor of 1000 the deviation of $eV_{oc\ loss}$ is within ≈0.2 eV in this region. When $E_{ICT+,D} \approx E_{ICT-,A}$ corresponding to the green region in Figure 3 a decrease in $V_{oc\ loss}$ is seen. This can be explained in terms of an ICT-induced dipole layer that assists in the dissociation of photogenerated CT-complexes into free charges,[26,27,40] leading to a dramatic increase of the fraction G/β in Equation 1.

To the left of the green region in Figure 3, an increased difference between $E_{ICT+,D}$ and $E_{ICT-,A}$ signifies an increased density of occupied ICT states (and interface potential step) at the bulk heterojunction interfaces that according to Equation 3 and Equation 4 cause an increased $V_{oc\ loss}$ due to the increased trap-assisted recombination ($n_s > 1$), which indeed is experimentally verified. Experimentally derived prefactors n_s obtained from literature are also shown in bottom panel of Figure 3. An increasing trend for n_s is found for blends with increasing Δ, while for blends with $\Delta = 0$ (to the right of the green region in Figure 3) bimolecular recombination, or $n_s = 1$, is found, in agreement with the model.

If our model holds, we expect the generation of ICT states when $E_{ICT+,D} \leq E_{ICT-,A}$. Photoinduced absorption (PA) measurements show that in rr-P3HT:$PC_{60}BM$ where $E_{ICT+,D} < E_{ICT-,A}$, we observe the presence of polarons in sub-gap photo-induced absorption (see Supporting Information Figure S7a). The presence of polarons in the sub-gap photo-induced absorption could either be due to ICT states or photogenerated CT states, however. Furthermore, we could expect a small density of ICT states at the bulk heterojunction for the D/A blends that feature $E_{ICT-,A} \approx E_{ICT+,D}$ as the absolute frontier of the respective ICT distributions may overlap. To be able to probe such small levels of ICT density and exclude contribution from photogenerated CT states we turn to electron paramagnetic resonance (EPR) measurements carried out in the dark. We choose here TQ1:$PC_{70}BM$ and TQ1:$PC_{60}BM$ blends (TQ1: poly[2,3-bis-(3-octyloxyphenyl)quinoxaline-5, 8-dilyl-alt-thiophene-2, 5-diyl]), as $E_{ICT-,A} \approx E_{ICT+,D}$ for these donor–acceptor combinations and due to the high purity of TQ1 as compared to rr-P3HT (see Section 2.4 of the Supporting Information). TQ1 is a donor polymer featuring comparatively high V_{oc} (0.89 V) and power conversion efficiencies (6%) when used in combination with $PC_{70}BM$.[41] Since $E_{ICT-,A} \approx E_{ICT+,D}$ there is no dipole at the D/A interfaces as measured by UPS. However, as the frontier edge of the respective ICT distributions likely will overlap, some integer charge transfer is still expected involving the most easily oxidized sites of the donor polymers and most easily reduced sites on the fullerene side of the heterojunction (see Figure S1 and the related discussion in the Supporting Information). The neat films of $PC_{60}BM$, $PC_{70}BM$ and TQ1 all show weak signals related to spin-carrying species, see **Figure 4** and Figure S8 (Supporting Information) for further details. The TQ1:$PC_{70}BM$ and TQ1:$PC_{60}BM$ blends, however, feature new and significantly stronger EPR signals with g-factors and linewidths that are different from those of the neat films (see Figure S8, Supporting Information). These new EPR signals are most easily seen by subtracting the individual contributions of TQ1 and the respective fullerene from the blend EPR spectra, see the lowest curves in Figure 4a,b. The appearance of such

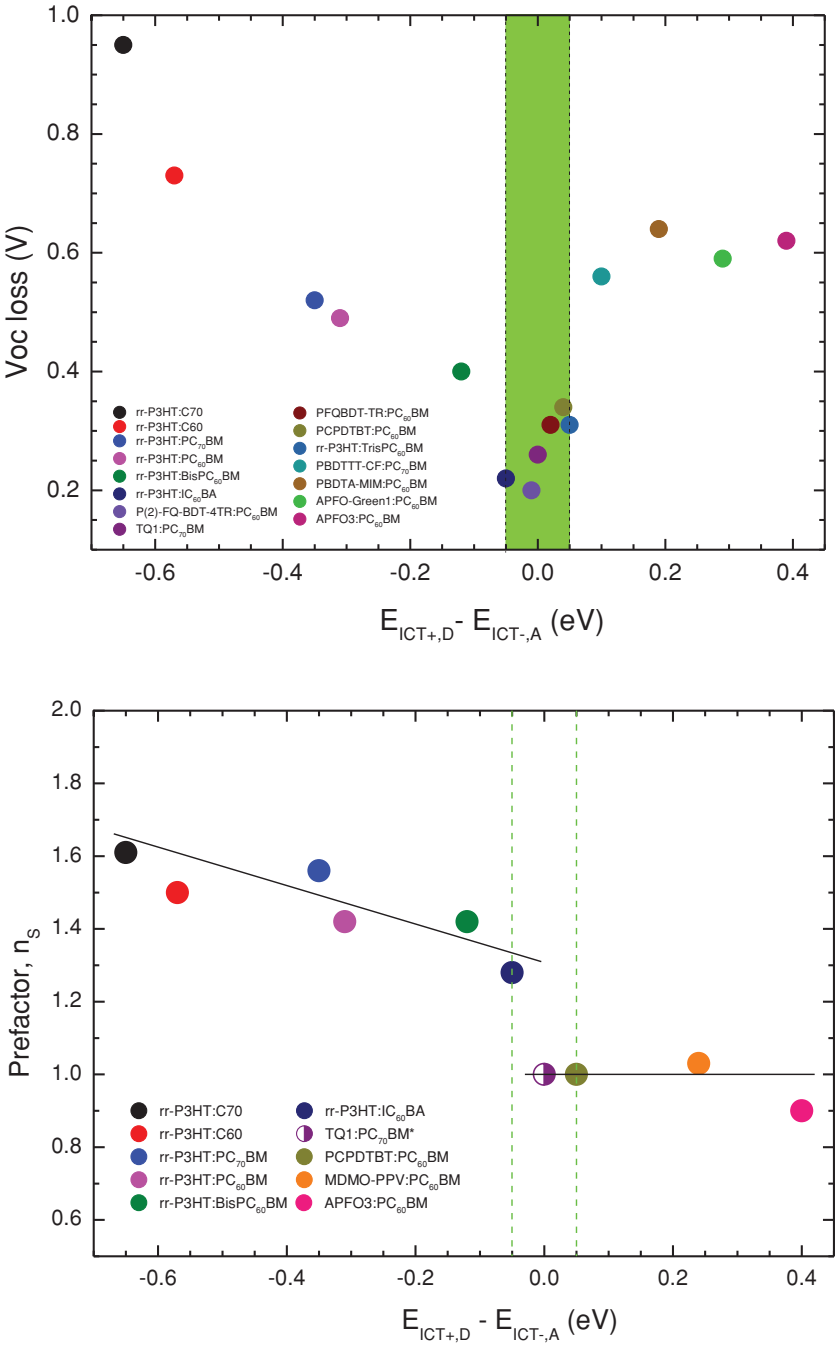

Figure 3. Top panel: $V_{oc\ loss} = \Delta E^{DA}_{g,eff} - V_{oc}$, plotted against the $E_{ICT+,D} - E_{ICT-,A}$ for a set of polymer:fullerene blends. The plotted data are given in Table S1 (Supporting Information). The green region contains the polymer:fullerene blends where $E_{ICT+,D} \approx E_{ICT-,A}$ within the error bar of the measurement. Bottom panel: The corresponding light-ideality factor n_s as a function of Δ for the rr-P3HT:fullerene series (see Table 1), PCPDTBT:$PC_{60}BM$[42] and $APFO_3$:$PC_{60}BM$.[43] We assign $n_s \approx 1$ for TQ1:$PC_{70}BM$, as it exhibits pure bimolecular recombination.[44] The n_s factor and $E_{ICT+,D}$ for MDMO-PPV:$PC_{60}BM$ are derived from literature.[40,45]

strong new EPR signals demonstrate that new spin-carrying species (polarons) are formed through integer charge transfer in the dark at the heterojunctions, that is, the formation of ICT states as predicted by the ICT model.

Thus a set of new design criteria using measured or calculated ICT states for BHJ solar cells can be proposed:

i) Pinned electrode contacts are obtained by: $\Phi_{anode} \geq E_{ICT+,D}$ and $\Phi_{cathode} \leq E_{ICT-,A}$;

ii)Donor:acceptor combinations should be chosen so that $E_{ICT-,A} \approx E_{ICT+,D}$.

3. Conclusion

We have studied that for a series of regioregular-poly(3-hexylthiophene):fullerene bulk heterojunction organic photovoltaic devices with pinned electrodes, integer charge transfer states present in the dark and created as a consequence of Fermi level equilibrium at BHJ have a profound effect on open circuit voltage. The donor ionization potential to acceptor electron affinity energy difference is thought to provide an upper limit to the V_{oc} in bulk heterojunction solar cells, but it is the effective energy gap including possible potential steps at the bulk heterojunction that is the relevant parameter. Here, the ICT state formation cause vacuum level misalignment that yields a roughly constant effective donor ionization potential to acceptor electron affinity energy difference at the donor–acceptor interface, even though there is a large variation in the fullerene series' electron affinity. We find that the large variation in open circuit voltage for the device series featuring different fullerenes instead is found to be a consequence of variations in trap-assisted recombination via ICT states, and show that this holds true regardless if one assumes a metal-insulator-metal or pn-junction based description of bulk heterojunction solar cells. EPR measurements confirm the creation of ICT states at the bulk heterojunctions in the dark and together with PA measurements show that the D/A coupling strength and recombination-induced loss can be estimated using the so-called pinning energies ($E_{ICT+,-}$). The results enable us to propose novel design rules for the donor/acceptor materials that hold the promise of in silico design of materials, as the these properties also can be calculated by for example, DFT-based methods: i) Pinned electrode contacts are obtained by: $\Phi_{anode} \geq E_{ICT+,D}$ and $\Phi_{cathode} \leq E_{ICT-,A}$, ii) Donor:acceptor combinations should be chosen so that $E_{ICT-,A} \approx E_{ICT+,D}$. The design rules are tested against a series of high performing donor polymers and their corresponding fullerene-based OPV devices available in literature, and excellent correlation is obtained.

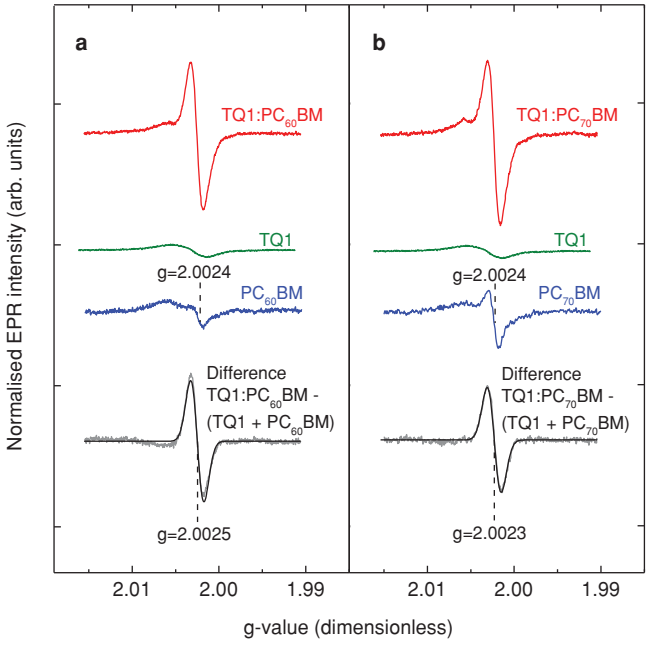

Figure 4. a) EPR spectra, volume normalized, of a TQ1:$PC_{60}BM$ 1:1 blend film (red), neat TQ1 (green) and $PC_{60}BM$ films (blue). The difference between the EPR spectrum of the blend and a sum of the neat TQ1 (green) and $PC_{60}BM$ (blue) film spectra are shown by the lowest curve (grey), representing new spin-carrying species created at the bulk heterojunction with a g-factor of 2.0025 that is different from those from the neat films (see Supporting Information Figure S8 for details). b) The corresponding EPR spectra of a TQ1:$PC_{70}BM$ 1:1 blend film, neat TQ1 (green), $PC_{70}BM$ film (blue) and difference spectrum (grey). All EPR spectra are volume normalized and vertically shifted for clarity.

4. Experimental Section

The fullerenes $C_{60/70}$ were obtained from Sigma Aldrich, and its derivatives $PC_{60/70}BM$, $BisPC_{60}BM$, $trisPC_{60}BM$ and $IC_{60}BA$ were purchased from Solenne BV. Polymer rr-P3HT was obtained from Sigma Aldrich, and PCPDTBT and PBDTTT-CF from One-Material. TQ1, P(2)-FQ-BDT-4TR, PFQBDT-TR1, PBDTA-MIM and APFO3 were synthesized at Chalmers University of Technology. All films were spin-coated from o-dichlorobenzene solutions and fabricated in a clean room, then directly transferred using a container covered with aluminum foil to shield from illuminations, into the load lock chamber of the ultrahigh vacuum (UHV) system used for measurement. Sets of conductive substrates were chose to provide a broad range of the work function: AlOx/Al dipped with NH3 solution ≈ 3.6–3.8 eV, ZnO nanoparticle film coated ITO ≈ 3.7–3.9 eV, AlOx/Al ≈ 3.8–4.0 eV, SiOx/Si ≈ 4.2–4.4 eV, AuOx/Au ≈ 4.3–4.7 eV, CuOx/Cu ≈ 4.4–4.5 eV, AgOx/Ag ≈ 4.5–4.6 eV, ITO and UVO treatment ≈ 4.6–4.9 eV, PEDOT:PSS ≈ 5.0–5.2 eV, and UVO treated AuOx/Au ≈ 5.3–5.9 eV. All substrates were cleaned by sonication in acetone and isopropyl before spin coating.

Ultraviolet Photoelectron Spectroscopy (UPS): UPS measurements were performed in an UHV surface analysis system including a sample analysis chamber with the base pressure of ≈ 2×10^{-10} mbar to characterize the work function of the substrates and fullerene films coated different substrates, respectively. UPS with HeI 21.22 eV as the excitation source was recorded with a Scienta-200 hemispherical analyzer, and calibrated by determining Fermi level edge of the Ar+ ion sputter-cleaned Au foil. The work function is derived from the secondary electron cut-off and the vertical ionization potential (IP) from the frontier edge of the occupied density of states.

Near-Edge X-Ray Adsorption Fine Structure (NEXAFS): NEXAFS spectra were performed at beam line D1011 of the MAX-II storage ring at the MAX lab, Sweden. The energy resolution was about 100 meV at photon energy close to the C K edge. NEXAFS spectra were collected in the partial electron yield mode by MCP with a different negative bias to screen the electrons with lower kinetic energy.

Photo-induced Absorption (PA): Samples for photo-induced absorption experiments were prepared from 25 mg/ml chlorobenzene solutions of polymers including regioregular poly(3-hexylthiophene) and TQ1 mixed with fullerene ($PC_{60}BM$, $PC_{70}BM$, $IC_{60}BA$) in 1:1 ratio by weight, by spincoating on sapphire substrates. Sample preparations were carried out in Nitrogen atmosphere. Annealing of the samples was performed on a hotplate at 120 °C for 15 min in Nitrogen atmosphere. For measurements, the sample was transferred to a cryostat (Janis Research), where it was kept under vacuum at room temperature (300 K). Photo-induced absorption was measured using either an Argon ion laser (Coherent Innova) for 514 nm (2.41 eV) excitation light (above-gap), or a diode laser (Power Technology) for 785 nm (1.58 eV) excitation light (below-gap). Both were set to an excitation intensity of 180 mW/cm^2. The excitation light was modulated by a mechanical chopper at 133 Hz. A tungsten projector lamp with appropriate cutoff filters served as probe light, which, after passing through the sample, was directed through a monochromator (Acton Research Corporation) and detected with Si, Ge and liquid nitrogen cooled InSb detectors and a lock-in amplifier (Stanford Research).

Electron Paramagnetic Resonance (EPR): EPR experiments were performed using a Bruker Elexsys E500 spectrometer operating at 9.88 GHz (X-band). All EPR spectra were obtained in dark and at room temperature. All blends were 1:1 by weight. All EPR spectra were normalized for film volume.

Supporting Information

Supporting Information is available from the Wiley Online Library or from the author

Acknowledgements

The work at Linköping University was sponsored by a project grant No 34142–1 from the Swedish Energy Agency and by the European Commission FP7 collaborative project SUNFLOWER (FP7-ICT-2011–7, Grant No. 287594). The work at Åbo Akademi University was supported in part by a project No.137093 (POHSC) from the Academy of Finland. X.L. and D.D. acknowledge support from The Swedish Research Council Linnaeus grant LiLi-NFM, while S.S. and R.Ö. acknowledge personal grants from the Waldemar von Frenckell Foundation and Swedish Cultural Foundation in Finland, respectively. S.B. acknowledges support from the Advanced Functional Materials Center at Linköping University.

Received: May 10, 2014
Revised: June 16, 2014
Published online: August 18, 2014

[1] Z. C. He, C. M. Zhong, S. J. Su, M. Xu, H. B. Wu, Y. Cao, *Nat. Photonics* **2012**, *6*, 591.
[2] J. You, L. Dou, K. Yoshimura, T. Kato, K. Ohya, T. Moriarty, K. Emery, C. C. Chen, J. Gao, G. Li, Y. Yang, *Nat. Commun.* **2013**, *4*, 1446.
[3] M. Helgesen, R. Sondergaard, F. C. Krebs, *J. Mater. Chem.* **2010**, *20*, 36.
[4] H. Jin, C. Tao, M. Velusamy, M. Aljada, Y. L. Zhang, M. Hambsch, P. L. Burn, P. Meredith, *Adv. Mater.* **2012**, *24*, 2572.
[5] J. Jo, S. S. Kim, S. I. Na, B. K. Yu, D. Y. Kim, *Adv. Funct. Mater.* **2009**, *19*, 866.
[6] Z. C. He, C. M. Zhong, X. Huang, W. Y. Wong, H. B. Wu, L. W. Chen, S. J. Su, Y. Cao, *Adv. Mater.* **2011**, *23*, 4636.

[7] H. Y. Chen, J. H. Hou, S. Q. Zhang, Y. Y. Liang, G. W. Yang, Y. Yang, L. P. Yu, Y. Wu, G. Li, *Nat. Photonics* **2009**, *3*, 649.
[8] B. Yang, Y. B. Yuan, P. Sharma, S. Poddar, R. Korlacki, S. Ducharme, A. Gruverman, R. Saraf, J. S. Huang, *Adv. Mater.* **2012**, *24*, 1455.
[9] C. J. Brabec, A. Cravino, D. Meissner, N. S. Sariciftci, T. Fromherz, M. T. Rispens, L. Sanchez, J. C. Hummelen, *Adv. Funct. Mater.* **2001**, *11*, 374.
[10] B. Yang, F. W. Guo, Y. B. Yuan, Z. G. Xiao, Y. Z. Lu, Q. F. Dong, J. S. Huang, *Adv. Mater.* **2013**, *25*, 572.
[11] J. Y. Yuan, Z. C. Zhai, H. L. Dong, J. Li, Z. Q. Jiang, Y. Y. Li, W. L. Ma, *Adv. Funct. Mater* **2013**, *23*, 885.
[12] M. D. Perez, C. Borek, S. R. Forrest, M. E. Thompson, *J. Am. Chem. Soc.* **2009**, *131*, 9281.
[13] K. Vandewal, K. Tvingstedt, A. Gadisa, O. Inganas, J. V. Manca, *Phys. Rev. B* **2010**, *81*, 8.
[14] W. Tress, K. Leo, M. Riede, *Appl. Phys. Lett.* **2013**, *102*, 163901.
[15] H. Ishii, K. Sugiyama, E. Ito, K. Seki, *Adv. Mater.* **1999**, *11*, 605.
[16] S. Braun, W. R. Salaneck, M. Fahlman, *Adv. Mater.* **2009**, *21*, 1450.
[17] M. Fahlman, P. Sehati, W. Osikowicz, S. Braun, M. P. de Jong, G. Brocks, *J. Electron Spectrosc. Relat. Phenom.* **2013**, *190*, 33.
[18] M. T. Greiner, M. G. Helander, W. M. Tang, Z. B. Wang, J. Qiu, Z. H. Lu, *Nat. Mater.* **2011**, *11*, 76.
[19] C. Tengstedt, W. Osikowicz, W. R. Salaneck, I. D. Parker, C.-H. Hsu, M. Fahlman, *Appl. Phys. Lett.* **2006**, *88*, 053502.
[20] L. Ley, Y. Smets, C. I. Pakes, J. Ristein, *Adv. Funct. Mater.* **2013**, *23*, 794.
[21] S. Braun, X. Liu, W. R. Salaneck, M. Fahlman, *Org. Electron.* **2010**, *11*, 212.
[22] G. Brocks, D. Cakir, M. Bokdam, M. P. de Jong, M. Fahlman, *Org. Electron.* **2012**, *13*, 1793.
[23] M. Fahlman, A. Crispin, X. Crispin, S. K. M. Henze, M. P. de Jong, W. Osikowicz, C. Tengstedt, W. R. Salaneck, *J. Phys. Condens. Matter Inst. Phys. J* **2007**, *19*, 183202.
[24] M. Bokdam, D. Cakir, G. Brocks, *Appl. Phys. Lett.* **2011**, *98*, 113303.
[25] D. Cakir, M. Bokdam, M. P. de Jong, M. Fahlman, G. Brocks, *Appl. Phys. Lett.* **2012**, *100*, 203302.
[26] H. Aarnio, P. Sehati, S. Braun, M. Nyman, M. P. de Jong, M. Fahlman, R. Osterbacka, *Adv. Energy. Mater.* **2011**, *1*, 792.
[27] V. I. Arkhipov, P. Heremans, H. Bassler, *Appl. Phys. Lett.* **2003**, *82*, 4605.
[28] B. C. Thompson, J. M. J. Frechet, *Angew. Chem. Int. Ed.* **2008**, *47*, 58.
[29] G. Dennler, M. C. Scharber, C. J. Brabec, *Adv. Mater.* **2009**, *21*, 1323.
[30] M. A. Faist, P. E. Keivanidis, S. Foster, P. H. Wobkenberg, T. D. Anthopoulos, D. D. C. Bradley, J. R. Durrant, J. Nelson, *J. Polym. Sci. Part B Polym. Phys.* **2011**, *49*, 45.
[31] Y. J. He, H. Y. Chen, J. H. Hou, Y. F. Li, *J. Am. Chem. Soc.* **2010**, *132*, 1377.
[32] M. Lenes, G. J. A. H. Wetzelaer, F. B. Kooistra, S. C. Veenstra, J. C. Hummelen, P. W. M. Blom, *Adv. Mater.* **2008**, *20*, 2116.
[33] V. D. Mihailetchi, P. W. M. Blom, J. C. Hummelen, M. T. Rispens, *J. Appl. Phys.* **2003**, *94*, 6849.
[34] S. K. M. Jonsson, E. Carlegrim, F. Zhang, W. R. Salaneck, M. Fahlman, *Jpn. J. Appl. Phys.* **2005**, *44*, 3695.
[35] A. Tada, Y. F. Geng, Q. S. Wei, K. Hashimoto, K. Tajima, *Nat. Mater.* **2011**, *10*, 450.
[36] L. J. A. Koster, E. C. P. Smits, V. D. Mihailetchi, P. W. M. Blom, *Phys. Rev. B* **2005**, *72*, 085205.
[37] A. Pivrikas, N. S. Sariciftci, G. Juška, R. Österbacka, *Prog. Photovolt: Res. Appl.* **2007**, *15*, 677.
[38] T. Kirchartz, B. E. Pieters, J. Kirkpatrick, U. Rau, J. Nelson, *Phys. Rev. B* **2011**, *83*, 115209.
[39] F. Deschler, E. D. Como, T. Limmer, R. Tautz, T. Godde, M. Bayer, E. v. Hauff, S. Yilmaz, S. Allard, U. Scherf, J. Feldmann, *Phys. Rev. Lett.* **2011**, *107*, 127402.
[40] P. Sehati, S. Braun, L. Lindell, X. J. Liu, L. M. Andersson, M. Fahlman, *IEEE J. Sel. Top. Quantum Electron.* **2010**, *16*, 1718.
[41] E. G. Wang, L. T. Hou, Z. Q. Wang, S. Hellstrom, F. L. Zhang, O. Inganas, M. R. Andersson, *Adv. Mater.* **2010**, *22*, 5240.
[42] G. A. H. Wetzelaer, M. Kuik, M. Lenes, P. W. M. Blom, *Appl. Phys. Lett.* **2011**, *99*, 153506.
[43] M. Nyman, personal communication.
[44] L. M. Andersson, A. Melianas, Y. Infahasaeng, Z. Tang, A. Yartsev, O. Inganäs, V. Sundström, *J. Phys. Chem. Lett.* **2013**, *4*, 2069.
[45] L. J. A. Koster, V. D. Mihailetchi, R. Ramaker, P. W. M. Blom, *Appl. Phys. Lett.* **2005**, *86*, 123509.
[46] T. Tromholt, M. V. Madsen, F. C. Krebs, *Appl. Phys. Lett.* **2013**, *102*, 123904.
[47] Z. L. Guan, J. B. Kim, H. Wang, C. Jaye, D. A. Fischer, Y. L. Loo, A. Kahn, *Org. Electron.* **2010**, *11*, 1779.
[48] H. Li, J. Z. Wang, *Appl. Phys. Lett.* **2012**, *101*, 263901.
[49] J. M. Ball, R. K. M. Bouwer, F. B. Kooistra, J. M. Frost, Y. B. Qi, E. B. Domingo, J. Smith, D. M. de Leeuw, J. C. Hummelen, J. Nelson, A. Kahn, N. Stingelin, D. D. C. Bradley, T. D. Anthopoulos, *J. Appl. Phys.* **2011**, *110*, 014506.
[50] H. Ohkita, S. Ito, *Polymer* **2011**, *52*, 4397.
[51] Z.-L. Guan, J. Bok Kim, Y.-L. Loo, A. Kahn, *J. Appl. Phys.* **2011**, *110*, 043719.
[52] G. Q. Ren, C. W. Schlenker, E. Ahmed, S. Subramaniyan, S. Olthof, A. Kahn, D. S. Ginger, S. A. Jenekhe, *Adv. Funct. Mater.* **2013**, *23*, 1238.
[53] K. Akaike, K. Kanai, H. Yoshida, J. y. Tsutsumi, T. Nishi, N. Sato, Y. Ouchi, K. Seki, *J. Appl. Phys.* **2008**, *104*, 023710.
[54] K. Kanai, K. Akaike, K. Koyasu, K. Sakai, T. Nishi, Y. Kamizuru, T. Nishi, Y. Ouchi, K. Seki, *Appl. Phys.* **2009**, *95*, 309.
[55] Y. Yang, F. Arias, L. Echegoyen, S. Flanagan, A. Robertson, L. J. Wilson, *Proc. Electrochem. Soc.* **1995**, *95–10*, 306.